



5-2013

Evaluation of the Transient Thermal Performance of a Graphite Foam/Phase Change Material Composite

Michael Paul Trammell
mtramme2@utk.edu

Follow this and additional works at: https://trace.tennessee.edu/utk_gradthes

 Part of the [Other Materials Science and Engineering Commons](#)

Recommended Citation

Trammell, Michael Paul, "Evaluation of the Transient Thermal Performance of a Graphite Foam/Phase Change Material Composite. " Master's Thesis, University of Tennessee, 2013.
https://trace.tennessee.edu/utk_gradthes/1689

This Thesis is brought to you for free and open access by the Graduate School at TRACE: Tennessee Research and Creative Exchange. It has been accepted for inclusion in Masters Theses by an authorized administrator of TRACE: Tennessee Research and Creative Exchange. For more information, please contact trace@utk.edu.

To the Graduate Council:

I am submitting herewith a thesis written by Michael Paul Trammell entitled "Evaluation of the Transient Thermal Performance of a Graphite Foam/Phase Change Material Composite." I have examined the final electronic copy of this thesis for form and content and recommend that it be accepted in partial fulfillment of the requirements for the degree of Master of Science, with a major in Materials Science and Engineering.

George M. Pharr, Major Professor

We have read this thesis and recommend its acceptance:

Claudia J. Rawn, James W. Klett

Accepted for the Council:

Carolyn R. Hodges

Vice Provost and Dean of the Graduate School

(Original signatures are on file with official student records.)

Evaluation of the Transient Thermal Performance of a Graphite Foam/Phase Change Material Composite

A Thesis Presented for the
Master of Science Degree
The University of Tennessee, Knoxville

Michael Paul Trammell

May 2013

Copyright © 2013 by Michael Paul Trammell

All rights reserved.

ACKNOWLEDGEMENT

First of all I wish to express my love and appreciation to my wife. Without her support and encouragement, this work would not have been possible. I also want to thank my parents Paul and Brenda Trammell for their inspiration and guidance.

I owe thanks to the members of my committee including Drs. G. M. Pharr, C. J. Rawn, and J. W. Klett for their teaching, guidance, advice, and encouragement.

In addition, I wish to express my continued gratitude to my colleagues Drs. T. D. Burchell and J. H. Miller for their mentoring and support.

I would like to express my appreciation to the Carbon Materials Group at Oak Ridge National Laboratory for providing essential facilities, materials, and equipment for this research.

ABSTRACT

The thermal transient response of graphite foam infiltrated with paraffin wax as a thermal protection composite was investigated. Graphite foam is a rigid open-celled porous carbon material that exhibits high thermal conductivity along the ligaments. To increase the ability of graphite foam to store heat energy, it was infiltrated with a phase change material, paraffin wax. Filling the foam with a phase change material (PCM) creates a composite that transfers heat through an interconnected network of ligaments to a large surface area of PCM for absorption. Foams were made at various pressures to understand the effect of porosity, which also controls infiltrated wax fraction, on the thermal performance of the composite. The foam samples were infiltrated with paraffin wax and tested using a constant temperature heat source. The transient response was recorded for each sample. The results indicate that a compromise exists between the heat absorption rate and the time available for protection. A simulation was also developed and agreed well with the experimental data.

TABLE OF CONTENTS

Chapter 1: Introduction	1
Chapter 2: Literature Review.....	3
Graphite Foam	3
Phase Change Material (PCM)	7
Thermal Performance Enhancing Composites.....	9
Numerical Studies	12
Chapter 3: Experimental Setup and Methodology	13
Test Equipment	13
Foam Production	18
Foam Samples	20
PCM Addition.....	21
Experimental Procedures	22
Chapter 3: Experimental Results and Discussion.....	23
Thermal Protection Potential	29
Chapter 4: Simulation	30
Software	30
Simulation Development	30
Simulation Optimization.....	34
Results and Discussion	35
Chapter 5: Conclusions and Recommendations	39
Bibliography	41
Appendix.....	44

Appendix A. Simulation Script.....	45
200 series simulation script.....	45
300 series simulation script.....	47
400 series simulation script.....	50
Vita	53

LIST OF FIGURES

Figure 1: SEM images of graphite foam (1)	5
Figure 2: Plane orientation due to volatile expansion.....	6
Figure 3: Graphitization of carbon as a function of temperature (6)	7
Figure 4: Schematic of experimental setup.....	14
Figure 5: Test container illustrating thermocouple placement	15
Figure 6: Thermocouple locations (inches) and identification	16
Figure 7: Test chamber with foam sample in place	17
Figure 8: Test chamber with foam sample and thermocouples in place.....	17
Figure 9: Test system including data acquisition units.....	18
Figure 10: Graphite foam samples showing varying pore size and structure	19
Figure 11: Graphite foam test sample.....	21
Figure 12: Experimental data from graphite foam without wax.....	24
Figure 13: Experimental data from wax filled composite samples.....	25
Figure 14: Experimental data for 200 series samples	26
Figure 15: Experimental data for 300 series samples	28
Figure 16: Experimental data for 400 series samples	29
Figure 17: Solid wax fraction as a function temperature for different ranges of melting	32
Figure 18: Simulation and experimental results of 200 psi foam/PCM composite	36
Figure 19: Simulation and experimental results of 300 psi foam/PCM composite	37
Figure 20: Simulation and experimental results of 400 psi foam/PCM composite	38

LIST OF TABLES

Table 1: Alkane Series Compounds and Properties (2)	9
Table 2: Sample Identification Matrix	20
Table 3: Foam Properties	34
Table 4: PCM Properties (2)	34

Chapter 1: Introduction

Heat generation has been a persistent challenge over a broad range of engineering applications extending from electronic devices to nuclear reactors. Many issues arise from either the sensitive nature of the components within a system (thermal protection) or the need to stabilize temperature through a series of high and low heat generation periods (thermal stabilization). In many cases the most prevalent challenge to overcome is the storage or removal of heat. For some applications where a cooling media is unavailable, a passive system that can store energy and release it at a later time is desirable. This research will study the thermal characteristics of a passive cooling composite material consisting of graphite foam and a phase change material (PCM) for such applications.

Graphite foam has a relatively high apparent thermal conductivity (182 W/m-K) (*1*) due to a highly ordered graphitic structure along the foam ligaments. Additionally, a large internal surface area is available due to an open cellular porous structure. This combination of physical properties and cellular structure has proven to be an excellent lightweight thermal management material for solutions that utilize a cooling media. However, for applications where no cooling media is available, the foam lacks a desirable thermal capability. With a low volumetric heat capacity, the material does not have the ability to store significant amounts of heat energy but quickly reaches equilibrium, suspending heat removal.

A phase change material, on the other hand, can have very different thermal properties. The desirable characteristic of a PCM, such as paraffin wax, is the ability to store large amounts of energy over an extended period of time by changing phases from solid to liquid. The disadvantage, however, is the low thermal conductivity (0.02 W/m-K

for paraffin wax) (2) of the material. Additionally, once it begins to melt, the liquid fraction between the heat source and the solid fraction acts as a low thermal conductivity barrier to heat transfer.

This research focuses on combining the two materials by infiltrating the graphite foam with paraffin wax to create a series of graphite foam/PCM composite samples of varying foam porosity. The graphite foam serves as a high thermal conductivity, open-celled, interconnected, structural material that wicks heat from the source to be protected to a large volume of paraffin wax where it is stored. A series of samples were evaluated experimentally, providing insight to the thermal characteristics of the composite and the effect porosity and PCM volume fraction have on performance.

Chapter 2: Literature Review

The following sections outline the literature regarding research conducted on graphite foam, phase change materials (specifically paraffin wax), various thermal performance enhancing composites, and recent relevant numerical studies.

Graphite Foam

Graphite foam is an open-celled carbon material that exhibits high thermal conductivity along the ligaments. Klett (3) has provided a detailed history of the evolution of carbon and graphite foams that will be summarized here. Initial reports as early as the 1940's outline the groundwork of the early developments in carbon foam. Researchers such as Sterling (4) reported on specific chemical compositions of phenol and aldehyde that can be used to produce a solid cellular structure. Results from this work showed that the spontaneous volatile evolution was not sufficient to produce the desired low density foam. By adding a simple heat treatment process, the increased rate of gas evolution provided a controlled process for the production of an expanded cellular thermosetting resin. In the late 1960's, Ford (5) carbonized these thermosetting organic foams in a simple heat treatment process to produce a cellular refractory carbon that could withstand much higher temperatures (up to 3300°F) than the original phenol-formaldehyde foams. It was also reported that either a carbon or graphite material could be obtained by controlling the heat treatment process.

Beginning in the 1970's and for the next several decades, much of the research focus was on producing low cost carbon foams by exploring alternative precursors and modifying processing conditions. One such organic precursor was pitch. Pitch is a carbonaceous by-product from the distillation of an organic precursor, typically coal tar

or petroleum, and is widely used as a binder in the densification of carbon composites and the production of extruded graphite electrodes (6). In the early 1990's, Hagar et al at the Wright Patterson Air Force Base (WPAFB) developed a method for producing carbon foams from a mesophase pitch. A mesophase pitch is a complex mixture of aromatic hydrocarbons that form unique pre-graphitic liquid crystals (3, 6). This method utilized a blowing technique that saturated the pitch with a blowing agent causing it to foam. This process also required an oxidative stabilization step to prevent the foam from melting during carbonization (3). In 1997, James Klett (7) at the Oak Ridge National Laboratory reported on a simplified process for the fabrication of mesophase pitch derived graphitic foams . This unique process eliminated the traditional blowing steps as well as the need for oxidative stabilization. Foams produced using the method exhibited high bulk thermal conductivities compared to earlier foams. Graphite foams produced by this method and used here exhibit a unique combination of physical properties due to a predominately open-cellular structure and highly ordered graphitic cell walls (Figure 1).

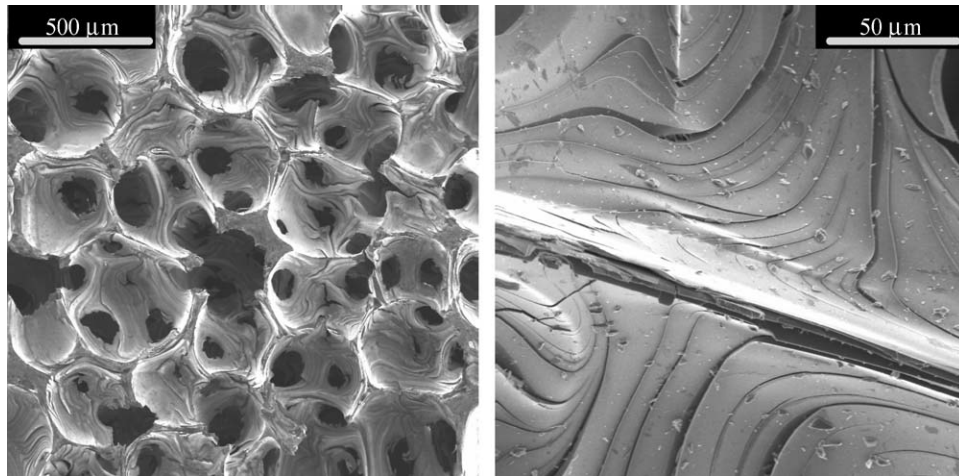


Figure 1: SEM images of graphite foam (1)

There are three key elements to consider when producing graphite foam: precursor, temperature, and pressure. All work dynamically allowing the foam structure and properties to be tailored to suit a large range of applications. Several precursors have been used to produce carbon foam in the past. For this research, the focus is on mesophase pitch derived foams as they provide the highest conductivity for thermal protection applications. To understand how these three elements provide variability, it is advantageous to describe the foaming process. A detailed explanation of this process and the fabrication of graphite foam is available (3) and will be summarized here.

Mesophase pitch is heated in a hot isostatic pressure (HIP) furnace under a predetermined positive pressure. As the temperature increases and the pitch melts, volatile materials begin to expand. The isostatic pressure is used to control this expansion thus controlling the pore size. Gas expansion in the melted pitch causes preferential orientation of the pre-graphitic crystals along the cell walls as illustrated in Figure 2.

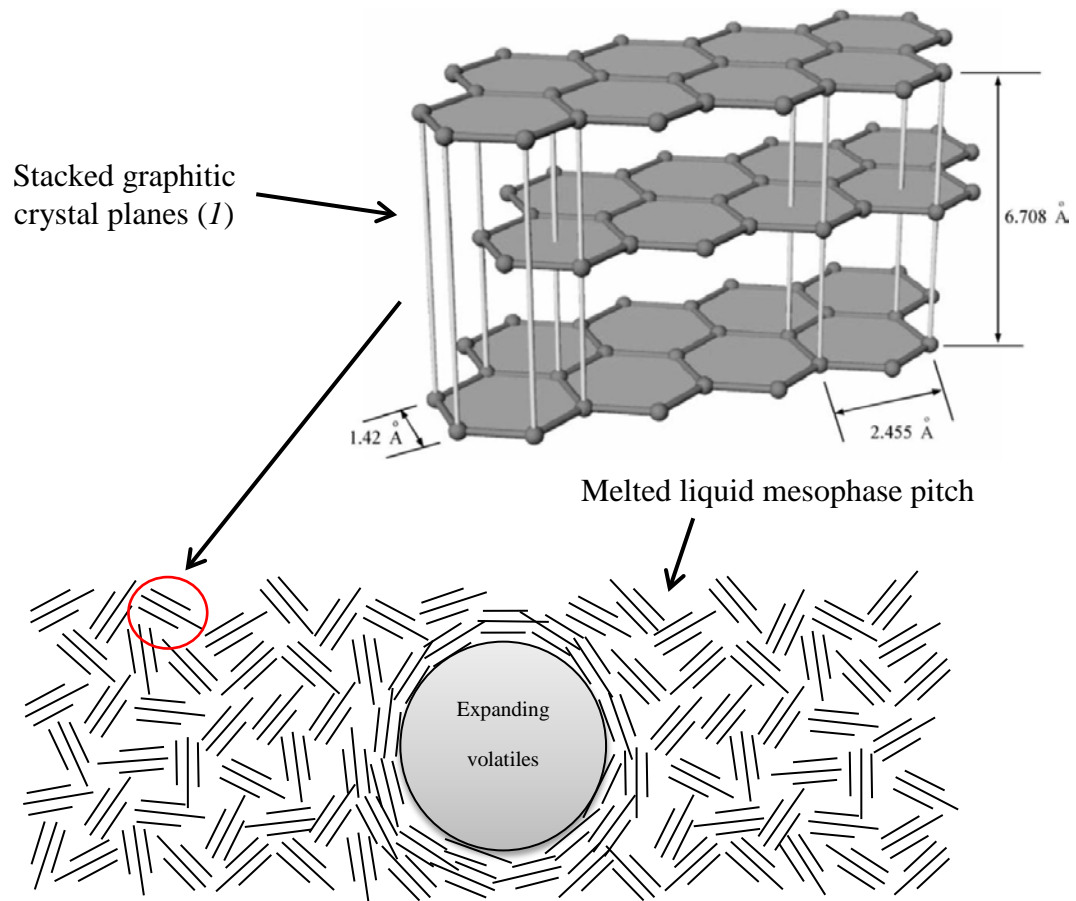


Figure 2: Plane orientation due to volatile expansion

As temperature increases further, the pitch hardens and captures the foam structure. Subsequent heat treatment is used to remove residual non carbon material (carbonization). At this point the foam is thermally insulating due to a slight misalignment of the graphitic crystal planes. Further heat treatment to a graphitizing temperature provides enough mobility for the graphitic planes to align (Figure 3) creating the highly ordered graphitic cell walls of the foam.

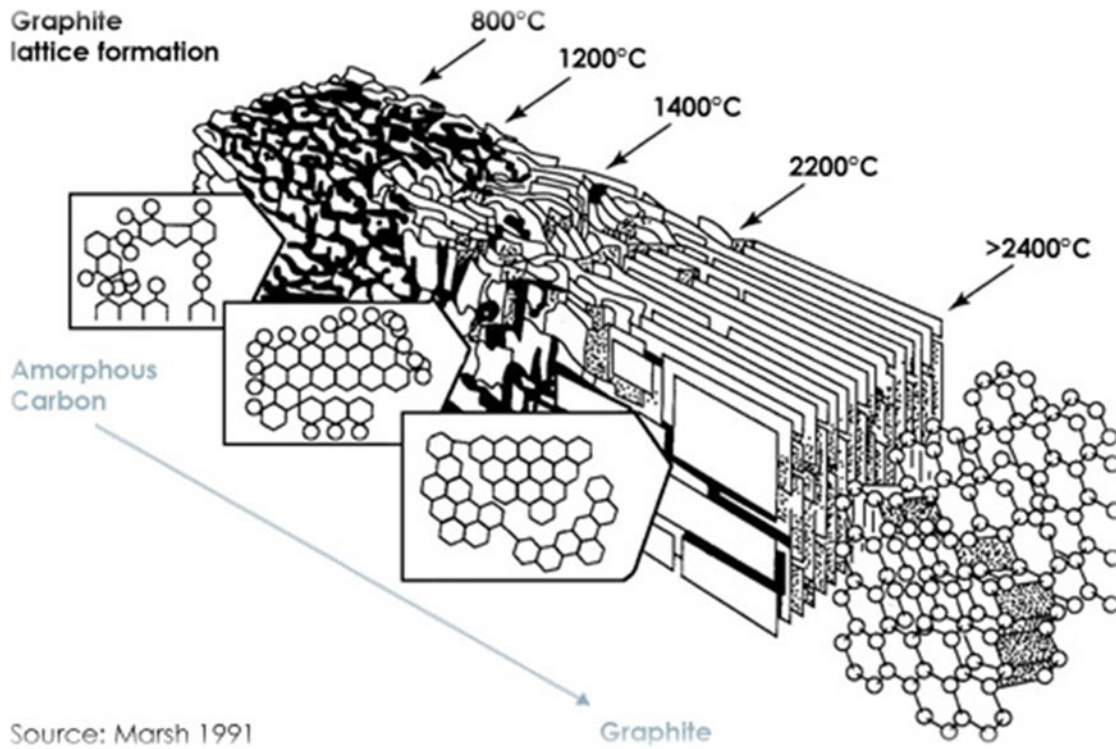


Figure 3: Graphitization of carbon as a function of temperature (6)

Although the specific foams produced in this report have lower values (40-60 W/m·K), with the optimal precursor and processing conditions, estimated ligament conductivities have been modeled to be greater than 1650 W/m·K with bulk conductivities up to 182 W/m·K (1).

Phase Change Material (PCM)

The phrase “phase change material” covers a vast class of materials including metals, hydrated salts, and waxes. These materials are widely used for thermal protection due to their ability to absorb large amounts of energy during the solid/liquid phase change. As the temperature of a PCM increases above the melting point, energy is stored as latent heat during the transition from solid to liquid and the source temperature is held

near the melting point. The stored energy can later be released as the PCM cools below the melting point and solidifies. PCM's typically exhibit low thermal conductivity and therefore are not desirable in applications where high rates of heat generation are expected.

For this research, the focus will be on paraffin wax as it offers a variety of advantages including low cost, chemical stability, high latent heat of fusion, and is available in a wide range of melting temperatures. Paraffin wax is a mixture of high molecular weight, straight chain, saturated aliphatic hydrocarbon compounds "alkane series" with the general formula (C_nH_{2n+2}) (8). As the "n" value in this formula, which indicates the number of carbon atoms "C" within the compound, increases, the melting temperature of the wax also increases providing the ability to match the melting temperature to a variety of applications. Table 1 lists various alkane series compounds and thermophysical properties including latent heat and melting temperatures.

Table 1: Alkane Series Compounds and Properties (2)

Name	No. of “C” Atoms	Melting Point (°C)	Density (kg/m ³)	Thermal Conductivity (W/mK)	Latent Heat (kJ/kg)
n - Dodecane	12	-12	750	0.21 ^S	n.a.
n - Tridecane	13	-6	756		n.a.
n - Tetradecane	14	4.5–5.6	771		231
n - Pentadecane	15	10	768	0.17	207
n - Hexadecane	16	18.2	774	0.21 ^S	238
n - Heptadecane	17	22	778		215
n - Octadecane	18	28.2	814 ^S [14], 775 ^L [14]	0.35 ^S [14], 0.149 ^L [14]	245
n - Nonadecane	19	31.9	912 ^S , 769 ^L	0.21 ^S	222
n - Eicosane	20	37			247
n - Heneicosane	21	41			215
n - Docosane	22	44			249
n - Tricosane	23	47			234
n - Tetracosane	24	51			255
n - Pentacosane	25	54			238
Paraffin wax	n.a.	32	785^S[15], 749^L[15]	0.514^S[15], 0.224^L[15]	251[15]
n - Hexacosane	26	56	770	0.21 ^S	257
n - Heptacosane	27	59	773		236
n - Octacosane	28	61	910 ^S , 765 ^L		255
n - Nonacosane	29	64			240
n - Triacontane	30	65			252
n - Hentriacontane	31	n.a.	930 ^S , 830 ^L		n.a.
n - Dotriacontane	32	70			n.a.
n - Tritriacontane	33	71			189

For economic reasons, paraffin wax is a mixture of many compounds from the alkane series and therefore does not have a distinct melting temperature (8). As the wax approaches the average melting temperature, some compounds begin to melt causing the material to soften. This can be described as a “mushy zone”. As the temperature increases further, other compounds begin to melt and the paraffin becomes liquid. This process also occurs in the reverse order as temperature decreases and the paraffin begins to solidify.

Thermal Performance Enhancing Composites

A phase change material alone would typically be useful only in applications where heat is generated slowly over a long period of time. By combining desirable thermophysical properties of multiple materials, composites become a viable solution for emergency thermal protection where heat is generated in relatively short pulses. Various

studies have been conducted on composite materials that utilize the high thermal storage capacity of paraffin wax by combining it with other materials selected specifically to enhance overall thermal performance.

Krishnan, et al, (9) reported on the effects of immersing the tip of a plate-fin heat sink in a phase change material. Convective cooling could take place over the exposed fin area when available. For high thermal loads and when convective cooling was not available, the PCM could absorb heat as a backup. Other material including carbon fibers (10, 11), which exhibit high thermal conductivity along the axis, aluminum powders (12), and graphite (13-15) have been used to enhance the thermal conductivity of paraffin wax. However, the non-interconnected material additions are still limited by heat transfer through the PCM from one element to another. Interconnected materials such as aluminum foams (16, 17) have similarly been combined with phase change materials to increase thermal performance. These materials typically exhibit lower apparent thermal conductivities than the bulk material due to reduction in density and add undesirable weight.

Graphite foam and paraffin wax composites for thermal protection have also been studied previously. Klett and Burchell (18) described a process for producing such composites by encasing the foam with phase change material creating a heat sink device. Graphite foam has an inherent advantage due a light weight interconnected network of high conductivity ligaments or struts that provide a characteristic high bulk thermal conductivity. This network can be attached directly to a heat source and allow heat to flow uninterrupted to a large area of phase change material.

A graphite foam/PCM composite can be tailored by varying the porosity in the foam. Porosity affects a host of properties such as density and thermal conductivity. Porosity also controls the wax fraction in the composite and thus dictates the overall thermal performance characteristics of the composite. In order to optimize the composite for a specific application, it is important to understand the relationship between porosity and thermal performance. In 2006 Mesalhy et al. (19) conducted an investigation of the effects of porosity and thermal properties on the thermal characteristics of graphite foam saturated with paraffin wax. In the study, disks were made of several types of commercially available foam from POCO Graphite, Inc. with varying properties and infiltrated with wax. The disks were placed in a Teflon cylinder with a copper heat source on top. Thermocouples recorded data as the samples were heated and temperature profiles were generated. The results indicated that thermal conductivity and pore size are the two main parameters in controlling heat source surface temperature. The sample with the large pore size and high conductivity produced the lowest surface temperatures but for a shorter time period indicating that a compromise exists between low surface temperatures and the time that a surface can be protected. Zhong et al. (20) observed a similar tradeoff by varying pore size and thermal properties of graphite foam/PCM composite. Their results showed that energy absorption via latent heat increased with an increasing mass fraction of PCM. More specifically, small pores resulted in higher diffusivities and larger pores yielded higher energy absorption values.

Since graphite foam has limited commercial availability, it is difficult to exclusively vary pores size while keeping other variables constant even if obtained from the same manufacturer. Therefore, in this experimental investigation, graphite foam

materials were produced in-house specifically for this study, thus allowing the production of various porosity foams while maintaining all other parameters such as precursors and production methods constant.

Numerical Studies

A significant amount of recent work focuses not only on the performance of a paraffin wax/PCM composite but also the modeling and prediction of thermal performance (19, 21, 22). Due to the complex random geometry of the graphite foam and the large difference between thermal characteristics of foam and paraffin wax, a detailed model is difficult to develop. However, some recent works have shown that simplified models are effective in predicting composite behavior (23-25). In this work, a simulation, based on some simplified assumptions, is used as a tool to provide close approximations of thermal performance based on composite geometry, individual material properties, and boundary conditions that approximate the experimental setup.

Chapter 3: Experimental Setup and Methodology

This section outlines the sample fabrication, experimental procedures, and test system used to investigate the thermal transient response of the graphite foam and graphite foam/PCM composite samples.

Test Equipment

The test system used in the experiments consists of several components that together make a controllable constant temperature thermal source that delivers heat to the center of a cylindrical test sample. Figure 4 shows a graphical representation of the elements described in this section. A temperature controlled water circulator (Lauda Brinkman RMS 6) delivers water at a constant temperature of 95°C through a loop of 0.5 inch stainless tubing. Stainless steel tubing is used to minimize heat loss as the water travels to the sample. The system utilizes a bypass that allows the water to circulate and reach the desired temperature while being isolated from the sample. The 6 inch section of thin wall (0.035") aluminum tubing that passes through the center of the sample acts as the heat source and is designed to create a slight pressed fit with the foam to maximize heat transfer.

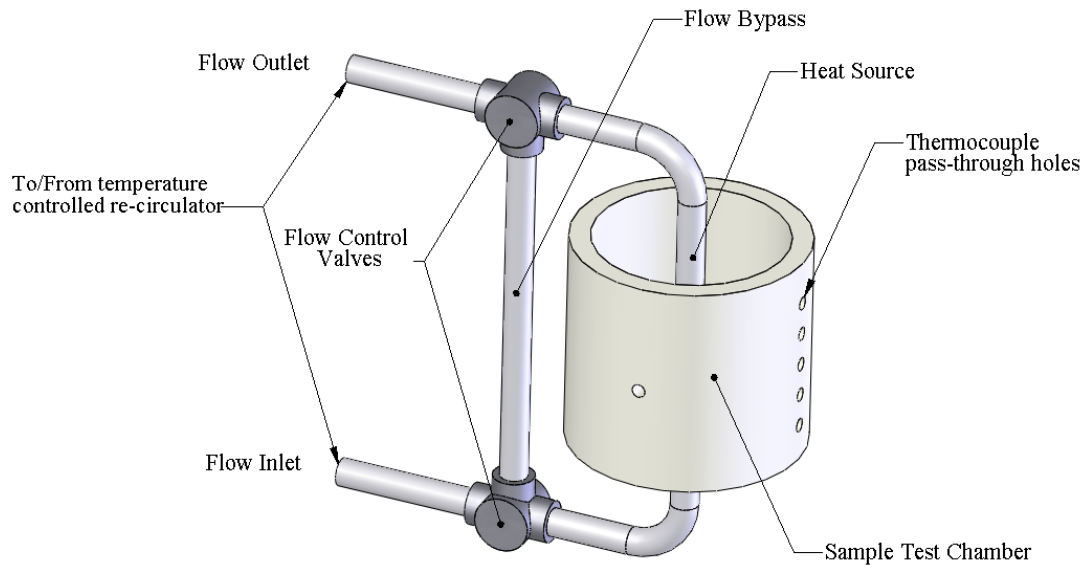


Figure 4: Schematic of experimental setup

A test chamber was designed to encapsulate the sample, provide containment for the paraffin wax, and insulate the boundary of the sample to minimize convective heat loss. The test chamber was machined from Teflon as it offers relatively low thermal conductivity and has low adhesion properties to allow for easy sample removal. The chamber is 0.25 inches thick on all surfaces and has a floating lid to accommodate expansion of the wax as it melts. SwagelokTM fittings were used to provide pass-through and precisely position thermocouples throughout the test sample. Figure 5 shows the test chamber with the thermocouples in place. Compression fittings were used to permanently attach the thermocouples insuring that data is taken at the same position for each sample. Five thermocouples were placed at incremental depths in the sample to acquire temperature profiles as the heat moves through the sample. Figure 6 illustrates the

dimensional positions of the thermocouple tips. Thermocouples were also placed at equal depths (axial center of sample) at four quadrants around the sample to verify symmetric heat flow. The inlet and outlet water temperatures were recorded as well as the outside temperature of the sample chamber.

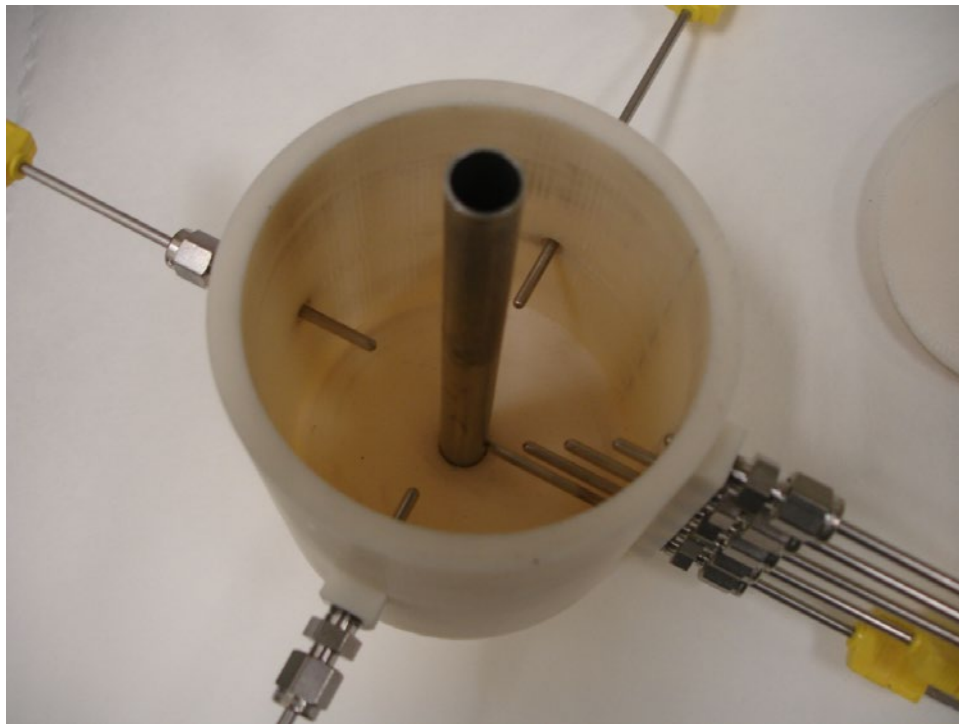


Figure 5: Test container illustrating thermocouple placement

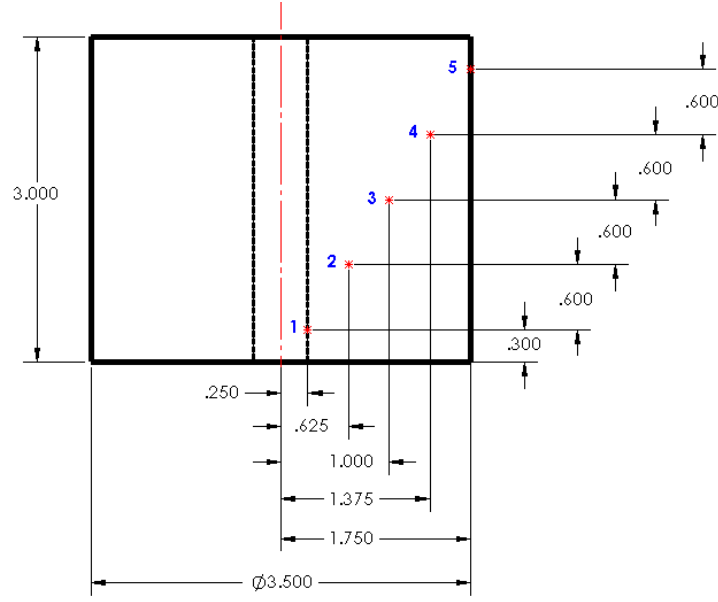


Figure 6: Thermocouple locations (inches) and identification

The 6 inch aluminum section of tube was slightly larger in diameter than a hole in the bottom of the chamber providing a pressed fit to secure and seal around the tube. Once the tube was in place, the foam sample was pressed into the chamber and around the inner tube (Figure 7). The thermocouples were then pressed into position piercing the foam sample. Figure 8 shows the foam sample and thermocouples in place. The thermocouples were identified to correspond with the appropriate data acquisition channels.



Figure 7: Test chamber with foam sample in place

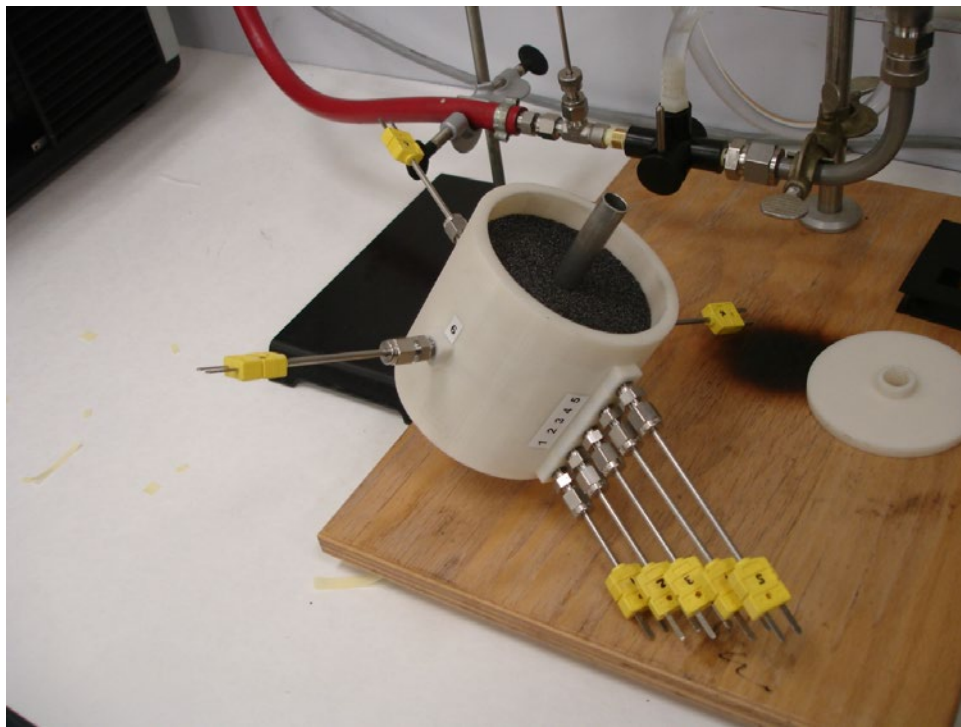


Figure 8: Test chamber with foam sample and thermocouples in place

Two Omega DAQ-PRO 5300 portable data acquisition units were used to take temperature data as a function of time from all thermocouples within the system. Fig 10 shows the assembled test system.

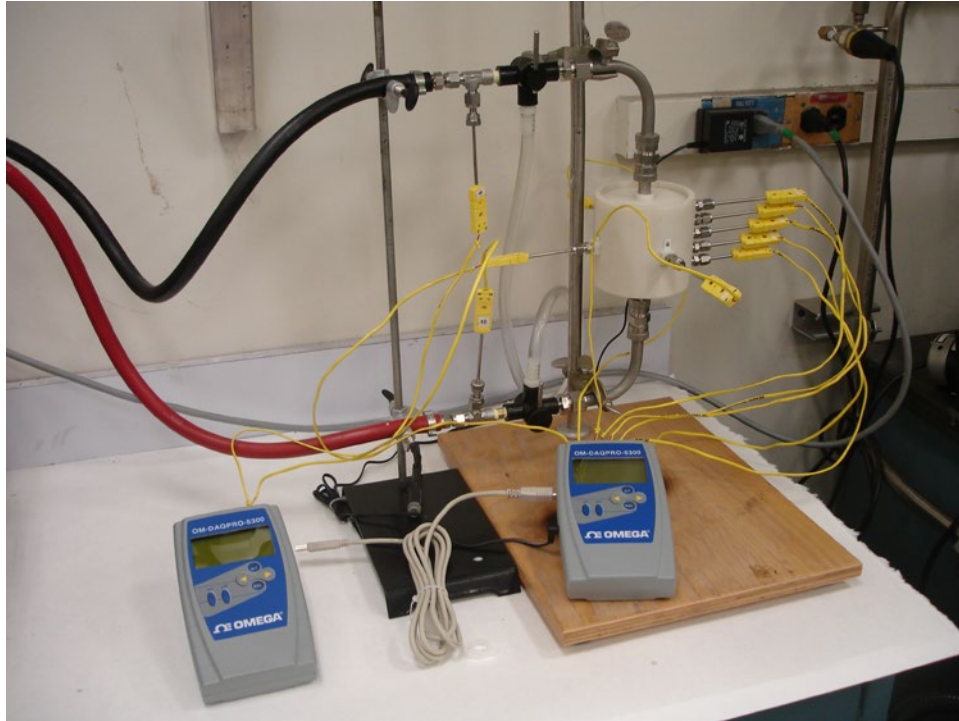


Figure 9: Test system including data acquisition units

Foam Production

Standard fabrication techniques were used to produce graphite foam in this research and will be briefly reviewed here (7). To provide a variation in porosity, three foaming runs were conducted at HIP pressures of 200, 300, and 400 psi with all other parameters such as composition and temperature held constant. This was achieved by loading a specific quantity of powdered mesophase pitch, supplied by KoppersTM,

material into 4" x 9" aluminum pans. After loading the pans, the pitch was covered with aluminum foil and loaded into a High temperature Isostatic Pressure (HIP) furnace. The pitch was heated under pressure to a temperature above the softening point. Once at the softening point, the material was allowed to foam for some time. The temperature was then raised to fuse the pitch and capture the foam geometry.

Once the foaming run was complete, the samples were carbonized by heating to 1000°C at a slow rate of 0.2 °C/minute in a nitrogen atmosphere to remove residual volatile materials. The slow heating rate for carbonization was necessary to allow sufficient time for volatile materials to escape and reduce cracking due to thermal stresses. At this point, the foams are insulating due to the lack of graphitic structure along the ligaments of the foam and need an additional heat treatment. A specialized furnace was used to heat the foam samples to 2800°C in nitrogen to promote graphitization. Figure 10 shows 0.75" diameter cored samples taken from the resulting foams and the variation in pore structure. Approximate void fractions (porosity) in the 200, 300, and 400 psi foams were 0.90, 0.88, and 0.83 respectively.

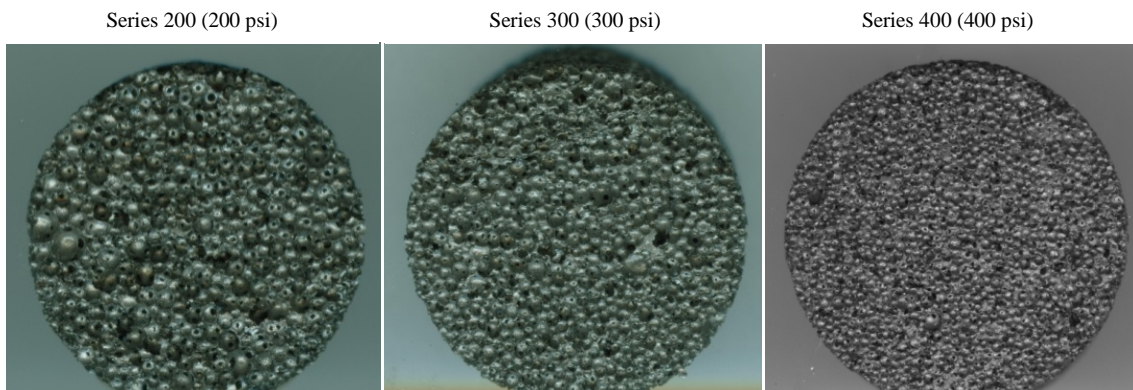


Figure 10: Graphite foam samples showing varying pore size and structure

Foam Samples

The initial step in sample preparation was to identify and produce usable samples from the raw foam material. The matrix in Table 2 provides identification for the three foam samples that were tested. Each foam sample was tested both with and without paraffin wax for a total of six test samples.

<i>Table 2: Sample Identification Matrix</i>		
Foam Series	Foam Only	Wax Filled
200	2XZ	2WZ
300	3XZ	3WZ
400	4XZ	4WZ

Cylindrical samples, one from each foam series, were machined from each billet as shown in Figure 11. These samples were 3 inches in diameter and 3.5 inches in height. A 0.5 inch diameter hole was cut through the center to allow for the placement of the 0.5 inch aluminum tube heating source.



Figure 11: Graphite foam test sample

PCM Addition

The foam-only samples were installed in the test chamber and tested prior to addition of the PCM. The PCM was added to the foam samples in the chamber so that the foam samples would not need removal from the chamber between tests. This ensured that thermal contact between the foam and the heat source was consistent between the foam-only and composite tests. After the initial foam-only test was complete, the sample was heated to a temperature slightly above the melting point of the wax using the same procedure as in testing. Once the sample was warm, wax that was pre-melted using a hot plate was poured into the foam until the top of the sample was reached. The low viscosity

of the melted wax insured that pores were sufficiently filled throughout the foam. The sample was allowed to cool to room temperature.

Experimental Procedures

The initial conditions for the experiment have the sample at room temperature and the water at the test temperature (95°C) flowing through the bypass. The test begins with a brief moment to record data at the initial conditions and the bypass valves are adjusted to direct the heated water through the tube in the center of the sample. The system is allowed to reach equilibrium. At the end of the test, the valves are switched back to redirect the heated water through the bypass. This is repeated for each sample configuration.

Chapter 3: Experimental Results and Discussion

Each graphite foam sample was first tested without wax to provide a baseline for comparison. After this, the foam was filled with wax as described in the previous section and retested. Data collection for all curves was taken at position 3 (P3), which is located in the center of the sample wall thickness. Figure 6 illustrates the thermocouple positions. Figure 12 is a plot of the transient temperature for each of the foam-only samples.

As expected, the graphite foam quickly (80°C within 125 seconds) approaches the temperature of the heat source due to the high thermal conductivity and low thermal mass of the sample. It was noticed that the equilibrium temperature of the 2XZ sample (lowest density) was much lower than expected. The expected equilibrium temperature for the sample in a well-insulated system should eventually approach an equilibrium temperature close to that of the heat source, even if the reduced thermal conductivity is considered

The lower than expected equilibrium temperature can be explained by several factors. Having the lowest density (highest porosity) makes this sample the most fragile allowing localized cracking of the foam and thus providing a non-ideal surface for contact with the heat source and thermocouples. The low amount of contact due to a damaged and porous surface could significantly overcome the relative high thermal conductivity of the foam and reduce overall heat transfer from the heat source to the sample.

The theory of a damaged contact interface could be confirmed by looking at the difference between inlet and outlet water temperatures. Unfortunately in this test system, the high flow of the water caused the inlet and outlet temperatures to be too close to measure a difference. Another option unavailable at the time of testing would be to

monitor the power output of the temperature controller. Reduced power of the temperature controller would indicate that heat was flowing into the sample at a much lower rate. This feature was not available at the time of testing.

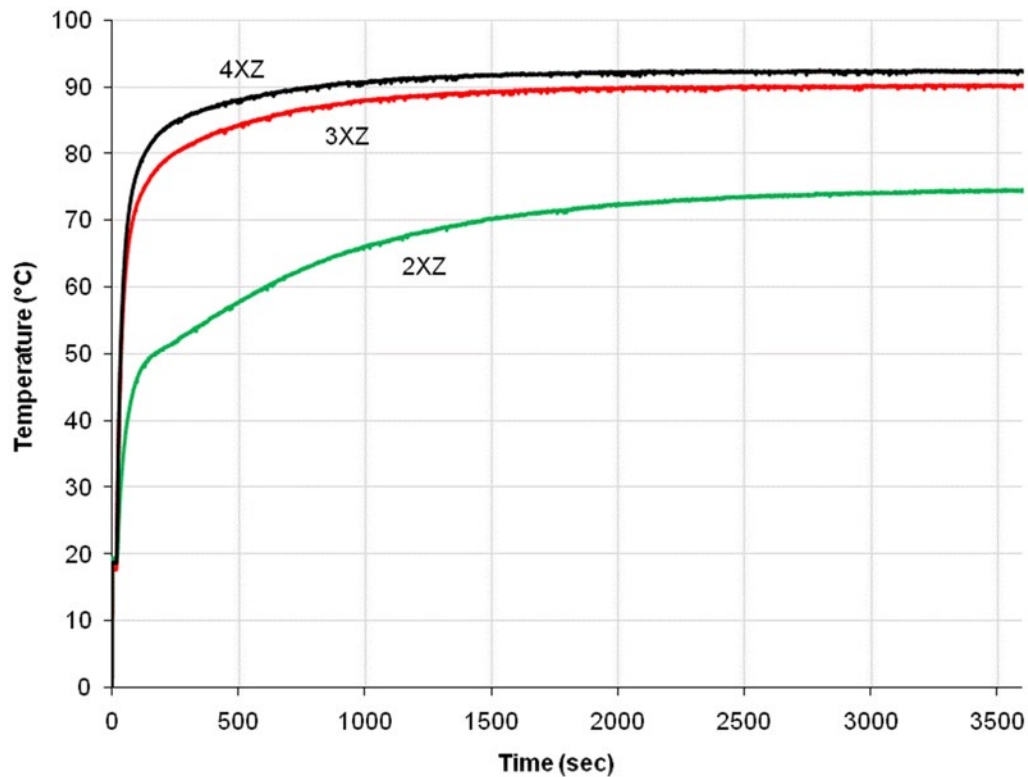


Figure 12: Experimental data from graphite foam without wax

After completing the test with the unfilled sample, wax was added and the test was repeated. The results in Figure 13 show how each wax filled sample compares relative to the change in foam density. As the composite sample temperature reaches the melting point of the wax, the rate of change in temperature decreases significantly. The

transition from heating to melting is controlled by the range in melting temperature of the wax. As discussed earlier, the wax used in this study melts over a range of temperatures. Depending on the melting range of the wax, this transition can be gradual to abrupt. The melting temperature range of the paraffin selected for this research gives a moderate transition with a range of 5-10°C.

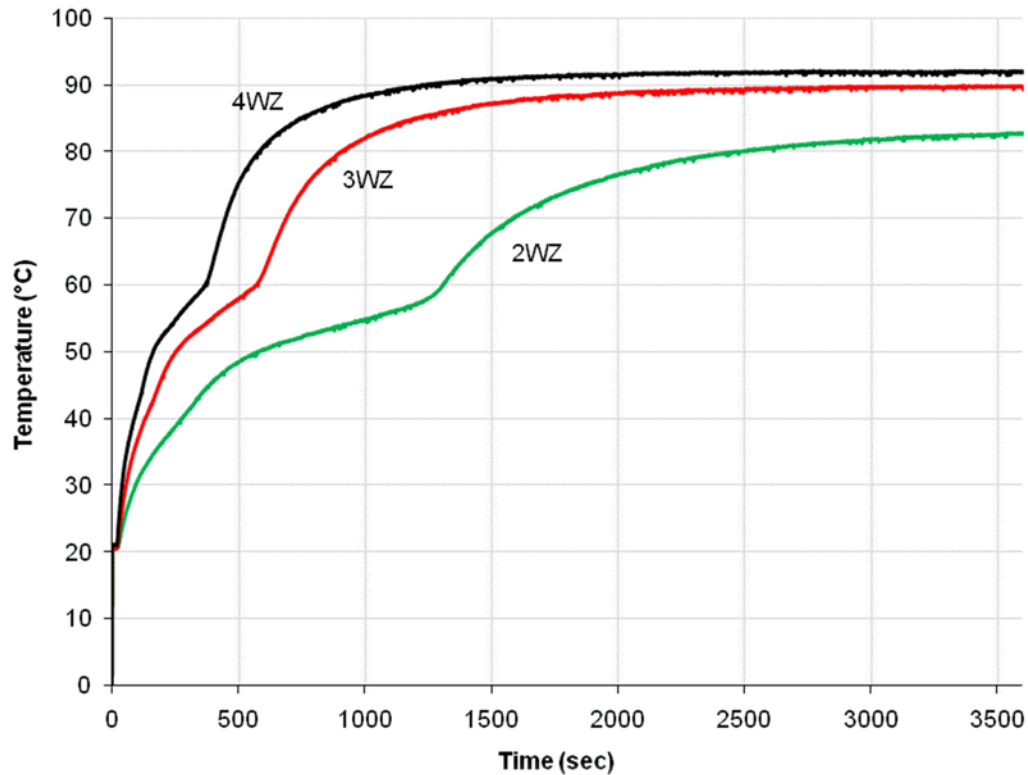


Figure 13: Experimental data from wax filled composite samples

To understand the advantage of infiltrating foam with paraffin wax, the following figures compare the composite samples to the respective “foam-only” baseline. In

comparing the 200 series samples, it is important to recall that 2XZ (foam-only) sample had an equilibrium temperature significantly lower than the heat source (20°C difference) due to poor contact at the interface between the sample and the heat source. In Figure 14, the equilibrium temperature of wax filled composite sample is actually higher than the baseline. This is most likely because the paraffin wax filling the gap between the foam and the heat source has a higher thermal conductivity than the air that was present during the foam-only test, thus allowing additional heat transfer to the sample.

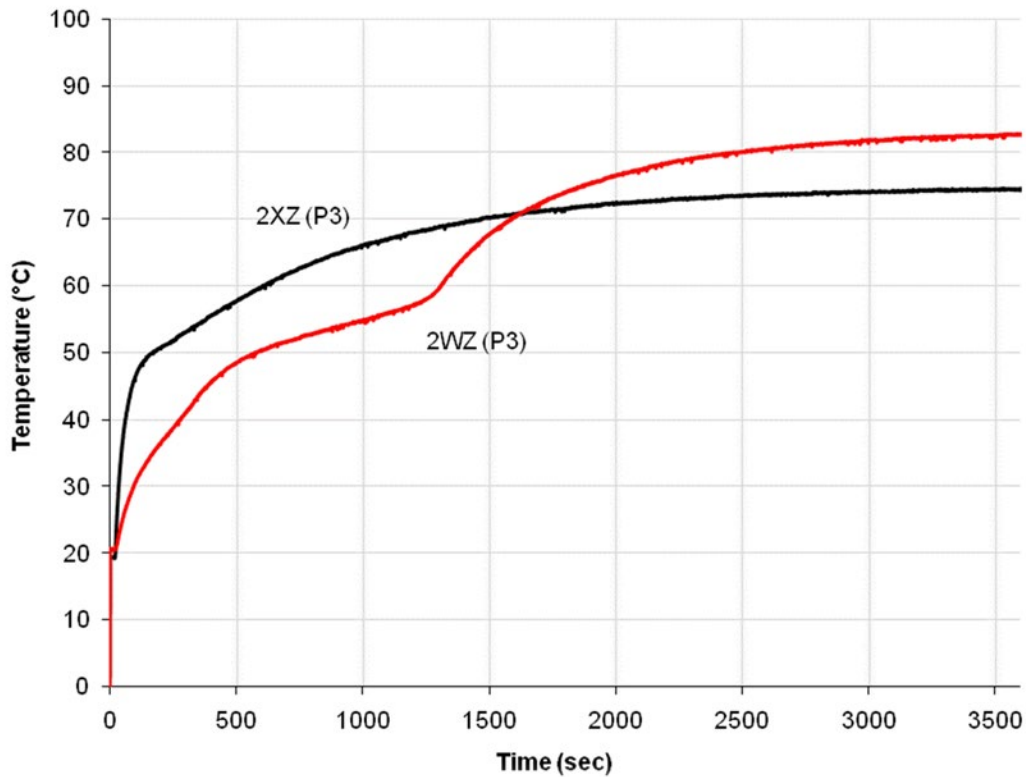


Figure 14: Experimental data for 200 series samples

Data from the 300 series samples (Figure 15) provides a much better look at the effect of wax infiltration on thermal performance. Looking at the data from a thermal protection perspective, the 3XZ (without wax) samples quickly reaches equilibrium with the heat source providing minimal protection. The wax filled sample (3WZ), on the other hand, provides thermal protection both prior to and during phase change. Early in the experiment (<250 seconds), the wax absorbs heat as the temperature rises. Near the paraffin melting temperature, the wax begins to change phase and absorb energy as latent heat thus reducing the rate at which temperature increases. The time elapsed while in this region is controlled by the amount of wax contained in the sample, which is in turn controlled by the porosity of the foam. This determines the amount of energy that can be absorbed before temperature begins to rise again. As the majority of the wax is melted, the second transition is observed where the sample begins to increase in temperature until equilibrium is reached.

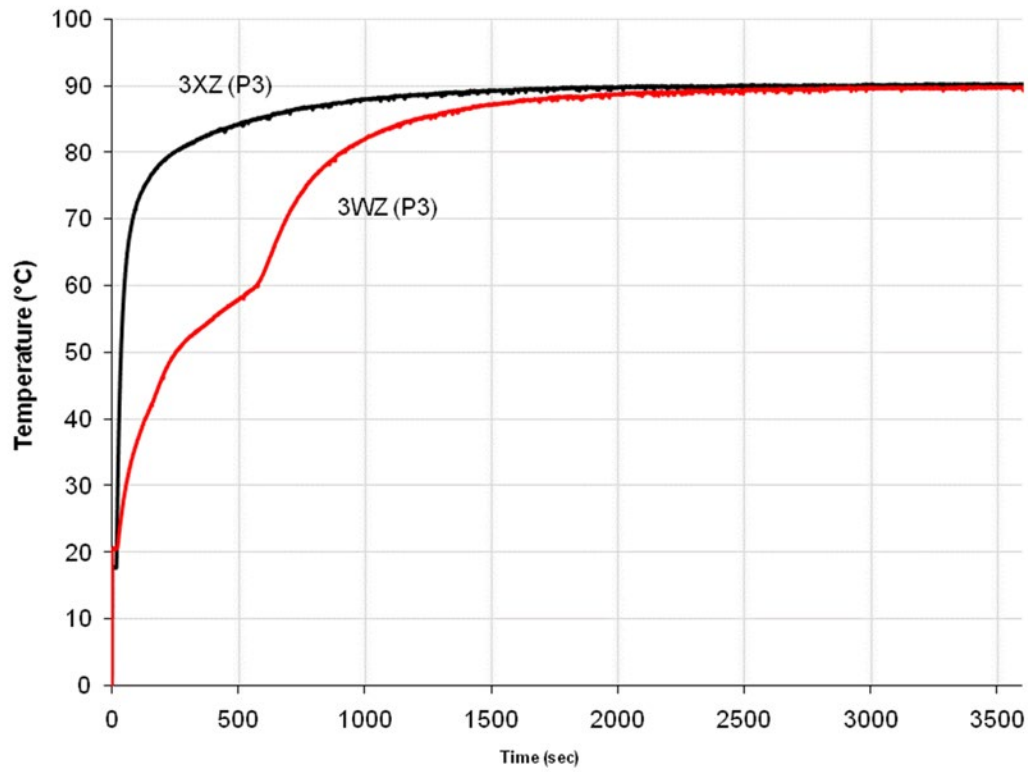


Figure 15: Experimental data for 300 series samples

Data from the 400 series samples (Figure 16) indicate a similar effect. However, the higher density 400 series foam has a lower porosity and a lower wax fraction for the composite sample. Comparing the curves from the 300 (3WZ) and 400 (4WZ) composite samples indicate a tradeoff that exists as a function of porosity. In other words, wax fraction increases with porosity. As the wax fraction changes, a compromise exists between the rate of heat absorption and the time heat can be absorbed.

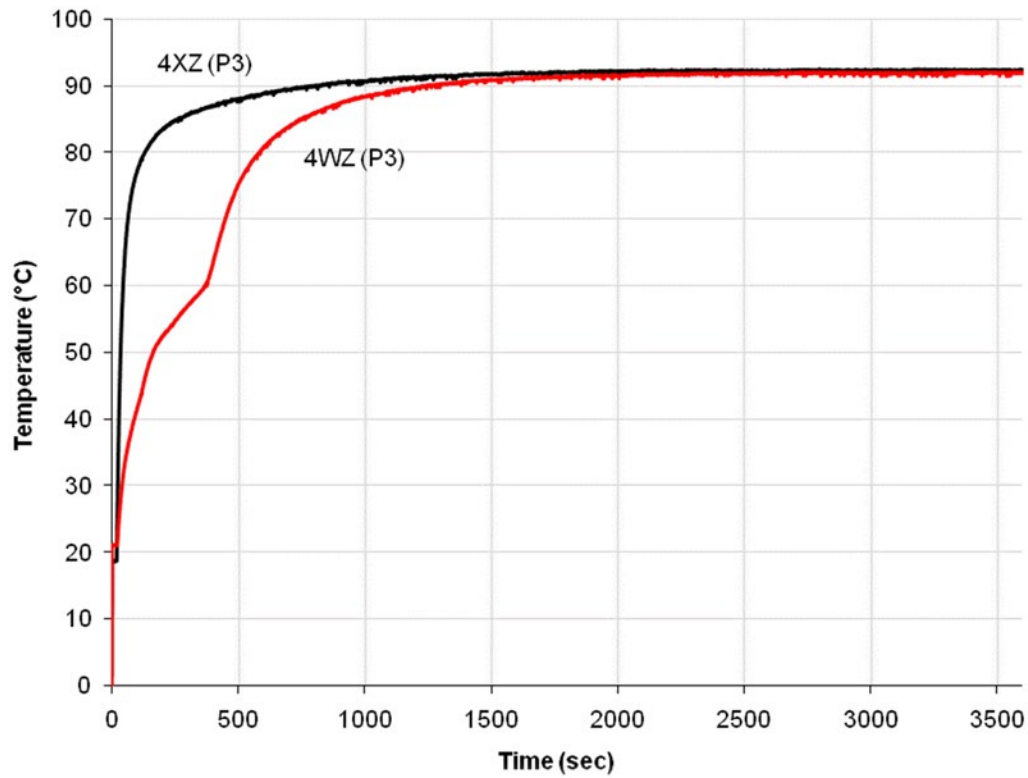


Figure 16: Experimental data for 400 series samples

Thermal Protection Potential

Comparing the results from the 300 and 400 series composite samples (Figure 13) offers an example of how a graphite foam/PCM composite material could be tailored for specific thermal protection application. Based on these results, if the desired protection temperature, heat generation rate and frequency are established, a composite material could be designed to provide optimized passive thermal protection.

Chapter 4: Simulation

Software

A computer simulation was developed using the partial differential equation solver FlexPDE (26). The software utilizes a pseudo code programming script and a library of built-in commands to create a geometrically representative model for finite element analysis. A partial differential equation can then be applied to the mesh and a solution is generated. The commercial software package was used to solve the heat equation based on the geometry, boundary conditions, and thermal conditions of the experimental study

Simulation Development

The initial steps of simulation development were to create a two dimensional representative geometry, generate a finite element mesh, and input boundary conditions. The boundaries were constructed using standard drawing commands. As the boundaries of the model were defined, the default built-in boundary condition equation was applied to the inner and outer surfaces of the sample. The default boundary condition assumes that heat flux is proportional to the temperature difference across the boundary interface and the proportionality constant is the inverse of the thermal contact resistance (26, 27). Since the thermal resistances at the inner and outer surfaces were unknown, they were used as the adjustable variable for refining boundary conditions to optimize simulation.

The foundation of the simulation centers on the general form of the heat equation (Equation 1) (27). The solution to this equation provides a temperature distribution as a function of time and position and it can be directly compared with experimental data.

$$\rho c_p \frac{\partial T}{\partial t} = \frac{\partial}{\partial x} \left(k \frac{\partial T}{\partial x} \right) + \frac{\partial}{\partial y} \left(k \frac{\partial T}{\partial y} \right) + \frac{\partial}{\partial z} \left(k \frac{\partial T}{\partial z} \right) + \dot{q} \quad \text{(Equation 1)}$$

Although the simulation assumes no internal heat generation, (\dot{q}) is used as a sink term to simulate the phase change process of paraffin wax in the composite. Equation 2 shows the sink term as a product of porosity (P), density (ρ), latent heat of melting (Q_m), and the change in solid wax fraction $\left(\frac{\partial S}{\partial t}\right)$. Note that the “S” refers to the solid fraction of partially melted wax and not entropy, which is typically standard in thermodynamic nomenclature.

$$\dot{q} = P \rho Q_m \frac{\partial S}{\partial t} \quad \text{(Equation 2)}$$

The change in solid wax fraction as a function of time, or $\left(\frac{\partial S}{\partial t}\right)$, is represented in Equation 3. The error function is used to simulate the kinetics of the solid to liquid phase transition (26) over the range of melting temperatures of the wax.

$$\frac{\partial S}{\partial t} = 0.5 \operatorname{erfc} \left(\frac{T - T_m}{T_r} \right) - S \quad \text{(Equation 3)}$$

As described previously, paraffin wax does not have a sharp melting temperature but instead melts over a temperature range. The input (T_r) controls the slope of the equation and is adjusted to simulate this range of temperature over which the wax melts. Increasing this value causes the simulated melting process to occur over a much broader

temperature range (Figure 17). The value of (T_r) used in the model was 10 based on the manufacturers melting range data.

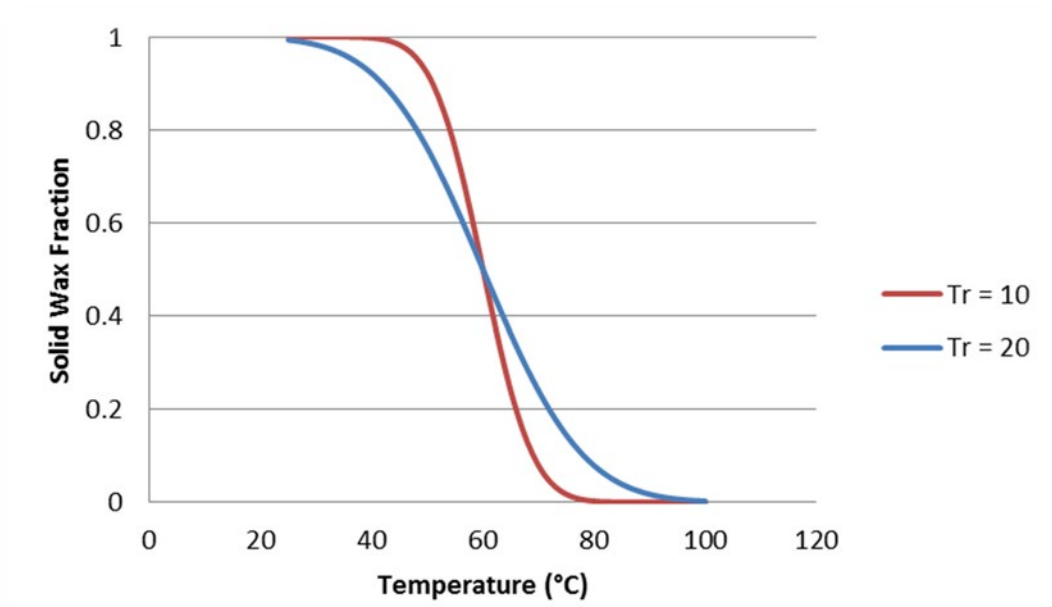


Figure 17: Solid wax fraction as a function temperature for different ranges of melting

As the composite reaches the melting temperature of the wax, energy is stored as latent heat. In Equation 3, the change in solid fraction ($\frac{\partial S}{\partial t}$) represents the amount of wax melted and becomes significant as the temperature (T) approaches the melting temperature (T_m) of the wax. In each time step within the model, the change in solid wax fraction is subtracted from the solid portion (S) in the previous time step (Equation 4). As the temperature rises above the melting temperature of the wax and the fraction of solid wax (S) approach zero, ($\frac{\partial S}{\partial t}$) becomes insignificant. As ($\frac{\partial S}{\partial t}$) becomes insignificant, the

sink term for the phase change in wax (Equation 2) also becomes insignificant allowing temperature to rise.

$$S_{new} = S_{old} - \frac{\partial S}{\partial t} \Delta t \quad \text{(Equation 4)}$$

Equations 1, 2, and 3 were combined and simplified to allow for easy implementation into the software script (Equation 5) (26).

$$\rho c_p \frac{\partial T}{\partial t} = \nabla k \nabla T + P \rho Q_m \left[0.5 \operatorname{erfc} \left(\frac{T - T_m}{T_r} \right) - S \right] \quad \text{(Equation 5)}$$

The general form of the heat equation includes material specific variables for density (ρ) and heat capacity (c_p). The product of these variables is volumetric heat capacity (ρc_p). Because the simulation does not account for the complex geometry of the individual composite constituent, the rule of mixtures was applied on a mass fraction basis to derive an effective volumetric heat capacity ($\rho c_{p,eff}$) for the composite. Equation 6 shows the effective volumetric heat capacity where (f_{pcm}) is the mass fraction of paraffin wax in the composite. This greatly simplifies the simulation by allowing the model to be treated as one material. The material property inputs used in this equation are listed in Table 3 and Table 4. For each sample configuration, a new script was developed with the appropriate inputs.

$$\rho c_{p,eff} = f_{pcm}(\rho c_{p,pcm}) + (1 - f_{pcm})(\rho c_{p,foam}) \quad \text{(Equation 6)}$$

Table 3: Foam Properties

Foam Series	Bulk Density (g/cm ³)	Porosity	Thermal Conductivity (W/mK)	Approximate Pore Size (μm)
200	0.22	0.90	40	1500
300	0.27	0.88	42	850
400	0.38	0.83	60	500

Table 4: PCM Properties (2)

PCM	Melting Point (°C)	Density (kg/m ³)	Thermal Conductivity (W/mK)	Latent Heat (kJ/kg)
Paraffin Wax	56*	785 ^S , 749 ^L	0.5 ^S , 0.2 ^L	251

* This melting point was taken from the manufacturers packaging.

Simulation Optimization

During initial simulation runs it was noticed that the thermal response of the 400 series composite exhibited the closest correlation with the simulation data. Therefore, the data from the 400 series foam experimental study were used as a baseline to optimize the simulation for all three foam series samples. Since the model assumes a thermal contact resistance at the inner and outer boundaries, the thermal contact resistance term was selected to adjust simulation results. The 400 series simulation results were refined by varying the boundary conditions for better agreement.

After boundary conditions were optimized for the 400 series case, those parameters were then applied to the 200 and 300 series simulations. After this optimization, the only difference between the 200, 300, and 400 series simulation were the material property inputs for thermal conductivity and porosity of the foam. Initial

conditions for the model were set to match the conditions in the experiment. This includes boundary conditions, heat source temperature, and geometry.

Results and Discussion

Each composite sample tested experimentally was modeled for a total of 3 simulations. Figure 18 shows the thermal response for the 200 series foam. This foam had the lowest density and was relatively fragile compared to the other samples. As mentioned previously, the 200 series foam did not make significant contact with the heat source. This caused the heat source controller to reduce power to maintain temperature thus reducing the heat into the sample. In turn, the sample did not reach the expected steady state temperature of the heat source. Since the model assumed perfect contact between the heat source and the composite sample, the model predicted the expected equilibrium temperature.

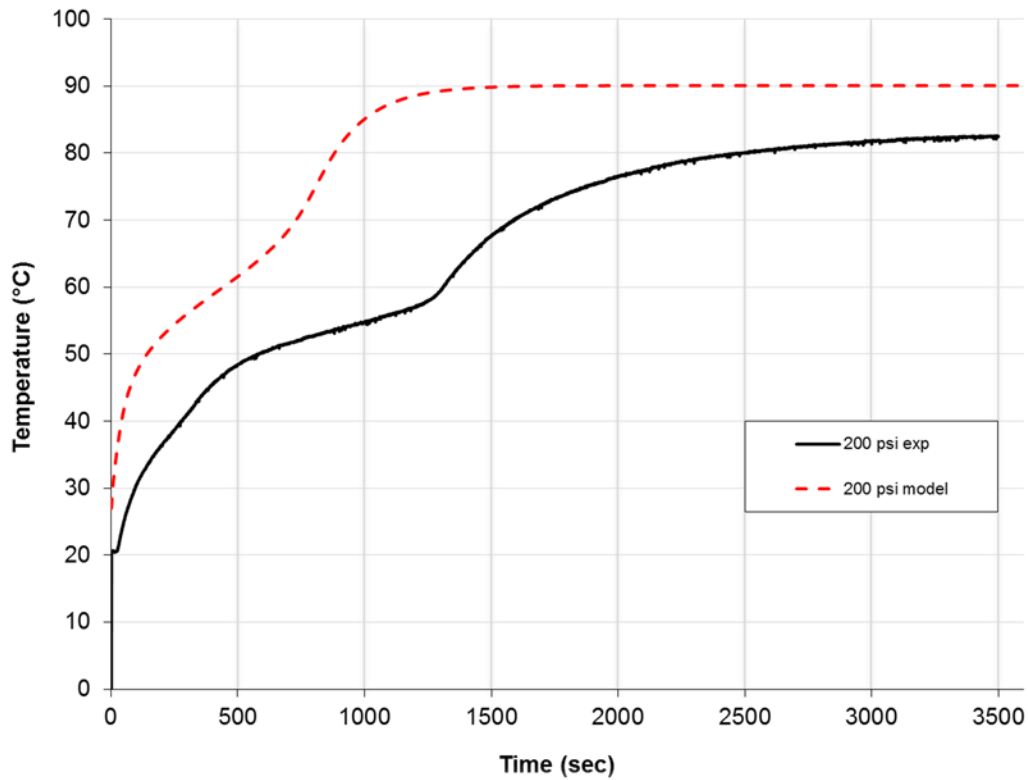


Figure 18: Simulation and experimental results of 200 psi foam/PCM composite

The 300 and 400 series foams were less fragile and made much better contact with the heat source. This is evident in the good agreement between experimental and simulated data seen in Figure 19 and Figure 20. Although the simulated data matches very well, it is difficult to accurately predict the phase change process. Several factors such as foam density gradient, wax motion, and heat loss contribute to the mismatched areas in the curve. The 400 series samples had the highest density and thus, the most rigid foam. The increased structural integrity resulted in a much better interface contact between the heat source and the sample. The smaller pores in the high density foam also

compartmentalized the wax and reduced the effect of convective heat transfer due to wax motion within the samples.

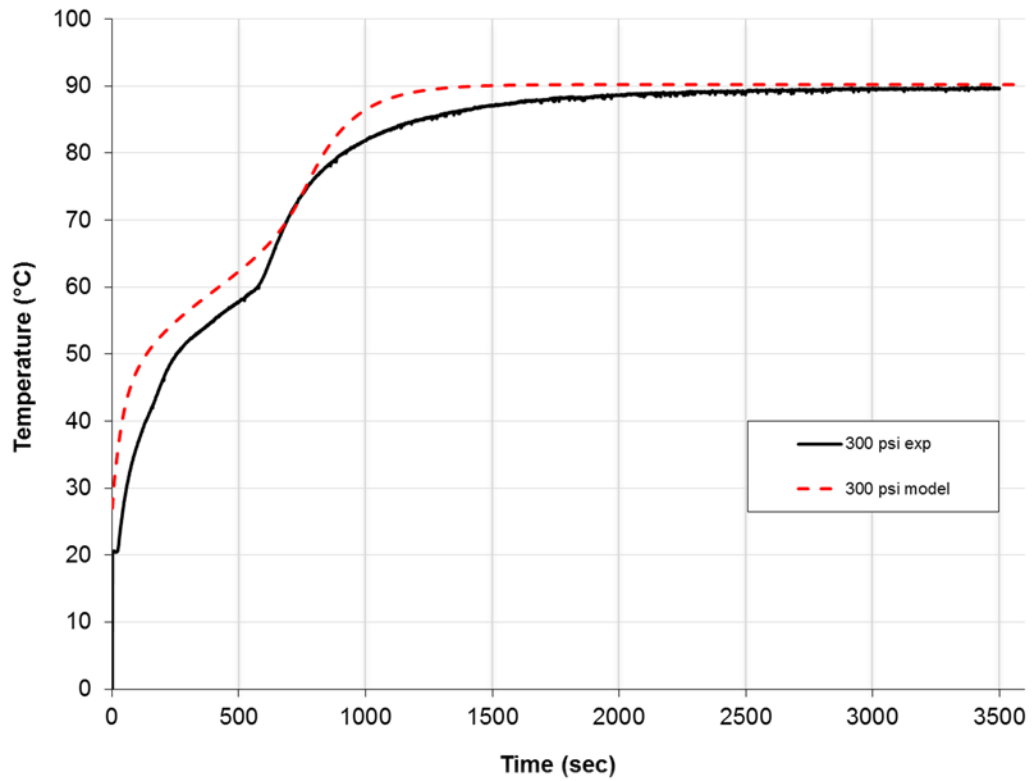


Figure 19: Simulation and experimental results of 300 psi foam/PCM composite

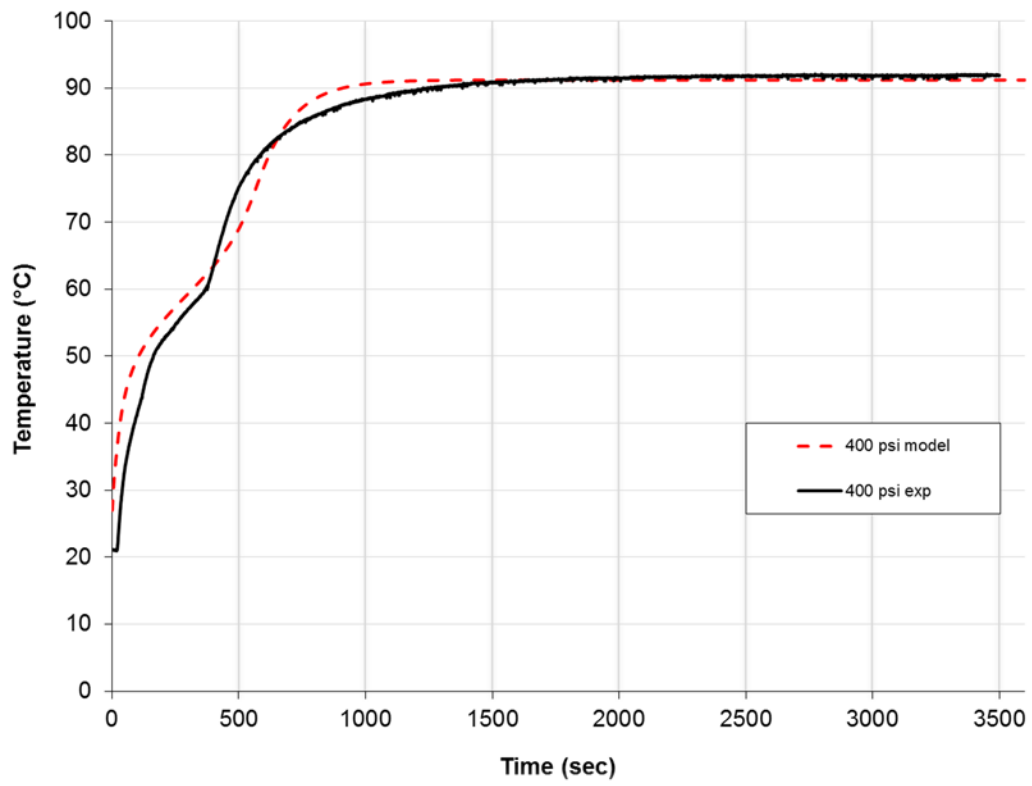


Figure 20: Simulation and experimental results of 400 psi foam/PCM composite

Chapter 5: Conclusions and Recommendations

A graphite foam/PCM composite material was investigated for thermal performance as a passive thermal protection material. As mentioned previously, foaming pressure during foam production controls pore size and thus a host of other properties such as density, thermal conductivity, and porosity. In this experiment, samples were machined from billets of graphite foam made at HIP pressures of 200, 300, and 400 psi. This gave three levels of foam density to investigate the effect of porosity on the thermal performance of the graphite foam as well as the composite (foam/PCM) material. The samples were tested without wax as a baseline and again after filling with wax. The results indicate a compromise that exists as a function of porosity. As the density increases in the graphite foam, the reduced porosity lowers the fraction of infiltrated wax in the composite samples. With lower fractions of wax, the composite absorbs energy (provides protection) at an increased rate but for less time. The experimental results suggest that if particular parameters are known about the system to be protected, a composite material could be tailored and optimized to provide passive thermal protection.

A simulation was developed using the commercial software FlexPDE. The partial differential equation solver provides a user-friendly interface for thermal performance analysis of a variety of samples configurations. Once the simulation was complete, it was used to estimate the transient thermal response of the varied porosity samples. Data from the simulation were then compared to experimental data. Although the 200 series samples provided limited data, the 300 and 400 series simulation data agreed well with the experimental results. The end result for the simulation is to allow a user to develop geometry, define boundary conditions, and input material properties for a specific

application and iteratively adjust sample parameters for thermal performance optimization of the composite.

Bibliography

1. Klett J. W., McMillan, A. D., Gallego, N. C., Walls, C. A., *J Mater Sci* **39**, 3659 (Jun 1, 2004).
2. Sharma S. D., Sagara, K., *Int J Green Energy* **2**, 1 (Jan-Mar, 2005).
3. Klett J., in *Cellular Ceramics : Structure, Manufacturing, Properties and Applications*, M. Scheffler, P. Colombo, Eds. (Wiley-VCH ; Chichester : John Wiley [distributor], Weinheim, 2005), pp. 137-157.
4. Sterling R., US Patent 2,629,698. 1949
5. Ford W., US Patent 3,121,050. 1964
6. Edwards I. A. S., in *Introduction to Carbon Science*, H. Marsh, Ed. (Butterworths, London ; Boston, 1989), pp. 1-36.
7. Klett J. W., US Patent 6,033,506. 2000
8. Garg H. P., Mullick, S. C., Bhargava, A. K., *Solar Thermal Energy Storage*. (D. Reidel Dordrecht, Holland, 1985), pp. 180.
9. Krishnan S., Garimella, S. V., Kang, S. S., *Ieee T Compon Pack T* **28**, 281 (Jun, 2005).
10. Frusteri F., Leonardi, V., Vasta, S., Restuccia, G., *Appl Therm Eng* **25**, 1623 (Aug, 2005).
11. Fukai J., Hamada, Y., Morozumi, Y., Miyatake, O., *Int J Heat Mass Tran* **45**, 4781 (Nov, 2002).
12. Mettawee E. B. S., Assassa, G. M. R., *Sol Energy* **81**, 839 (2007).
13. Mills A., Farid, M., Selman, J. R., Al-Hallaj, S., *Appl Therm Eng* **26**, 1652 (Oct, 2006).
14. Pincemin S., Olives, R., Py, X., Christ, M., *Sol Energ Mat Sol C* **92**, 603 (Jun, 2008).
15. Py X., Olives, R., Maurant, S., *Int J Heat Mass Tran* **44**, 2727 (Jul, 2001).
16. Hong S. T., Herling, D. R., *Scripta Mater* **55**, 887 (Nov, 2006).
17. Lafdi K., Mesalhy, O., Shaikh, S., *J Appl Phys* **102**, (Oct 15, 2007).
18. Klett J. W., Burchell, T. D., US Patent 6,780,505 B1. 2004
19. Mesalhy O., Lafdi, K., Elgafy, A., *Carbon* **44**, 2080 (Aug, 2006).

20. Zhong Y. J., Guo, Q. G., Li, S. Z., Shi, J. L., Liu, L., *Sol Energ Mat Sol C* **94**, 1011 (Jun, 2010).
21. Lafdi K., Mesalhy, O., Elyafy, A., *Carbon* **46**, 159 (Jan, 2008).
22. Mesalhy O., Lafdi, K., Elgafy, A., Bowman, K., *Energ Convers Manage* **46**, 847 (Apr, 2005).
23. Harris R., Leland, Q., Du, J., Chow, L. C., paper presented at the 9th AIAA/ASME Joint Thermophysics and Heat Transfer Conference, San Francisco, CA, 2006.
24. Wierschke K. W., Franke, M. E., Watts, R., Ponnappan, R., *J Thermophys Heat Tr* **20**, 865 (Oct-Dec, 2006).
25. Wirtz R. *et al.*, *AIAA Paper* **513**, (2003).
26. FlexPDE, "A Flexible Solution System for Partial Differential Equations", Version 5.0.11, www.pdesolutions.com, PDE Solutions Inc.
27. Incropera F. P., De Witt, D. P., *Fundamentals of Heat and Mass Transfer*. (Wiley, New York, ed. 3rd, 1990), pp. 919.

Appendix

Appendix A. Simulation Script

200 series simulation script

TITLE

'Foam/PCM Composite'

COORDINATES

ycylinder('r','z')

SELECT

cubic

smoothinit

VARIABLES

temp(threshold=10)

solid(threshold=0.1)

DEFINITIONS

long = 0.0762	{ height of cylinder }
dtube = .0127	{ diameter of inner tube }
dia = 0.0889	{ diameter of foam/pcm }
ta=300	{ outside air temperature }
Qm= 251000	{ latent heat of the PCM J/kg }
Tm=329	{ Melting temperature }
T0= 10	{ Melting interval +- T0 }
temp_liq=300	{ initial liquid temperature }
temp_sol=300	{ initial solid temperature }
lambda = 40	{ Thermal Conductivity of the foam }
e=0.90	{ Porosity }
filled=1	{ fraction filled }
rhopcm=760	{ Density pcm kg/m3 }
cppcm=2000	{ heat capacity pcm - J/kg--°C }
rhof=2200	{ Density solid ligaments of the foam - kg/m3 }
cpf=900	{ heat capacity -Foam -J/kg--°C }

$r_{\text{ceff}} = (e * \text{filled}) * (\rho_{\text{pcm}} * c_{\text{ppcm}}) + (1 - (e * \text{filled})) * (\rho_{\text{f}} * c_{\text{pf}})$ {effective heat capacity}
 $\rho_{\text{heff}} = (e * \text{filled}) * (\rho_{\text{pcm}}) + (1 - (e * \text{filled})) * (\rho_{\text{f}})$ {effective density}

INITIAL VALUES

temp=ta
 solid = $0.5 * \text{erfc}((\text{temp} - T_m) / T_0)$

EQUATIONS

temp: $r_{\text{ceff}} * \text{dt}(\text{temp}) - \text{div}(\lambda * \text{grad}(\text{temp})) = (e * \text{filled}) * \rho_{\text{pcm}} * Q_m * \text{dt}(\text{solid})$
 solid: $\text{dt}(\text{solid}) = 100 * (0.5 * \text{erfc}((\text{temp} - T_m) / T_0) - \text{solid}) + 1e-8 * \text{div}(\text{grad}(\text{solid}))$

BOUNDARIES

region 'Outer'

start 'outer' (0,-dia/2)
 natural(temp)=-10*(ta-temp) {outer surface convection}
 arc(center=0,0) angle 180

 natural(temp)=0 {cut line insulated}
 line to (0, dtube/2)

 natural(temp) = -24000*(368-temp)
 arc(center=0,0) angle=-180

 natural(temp)=0
 line to close

 FRONT(solid-0.5, 0.2)
 TIME 0 by 1e-4 to 3600

MONITORS

for cycle=1
 grid(r,z) zoom (0,-dtube,dtube,dtube)
 elevation(Temp) from (dtube/2,0) to (dia/2,0) fixed range=(300,370) as "X-Axis Temp"
 elevation(solid) from (dtube/2,0) to (dia/2,0) as "X-Axis Solid"
 elevation($r_{\text{ceff}} * \text{dt}(\text{temp})$, $\text{div}(\lambda * \text{grad}(\text{temp}))$, $\rho_{\text{heff}} * Q_m * \text{dt}(\text{solid})$) from (dtube/2,0) to (dia/2,0)

PLOTS

for cycle=10

grid(r,z)

contour(temp) fixed range=(300.0,370.0) painted

contour(temp) zoom (0,-dtube,dtube,dtube) fixed range=(300.0,370.0) painted

contour(solid) fixed range=(0.0,1.0) painted

contour(solid) zoom (0,-dtube,dtube,dtube) fixed range=(0.0,1.0) painted

grid(r,z) zoom (0,-dtube,dtube,dtube)

elevation(Temp) from (dtube/2,0) to (dia/2,0) fixed range=(300,370) as "X-Axis Temp"

elevation(solid) from (dtube/2,0) to (dia/2,0) as "X-Axis Solid"

elevation(rceff*dt(temp), div(lambda*grad(temp)), (e*filled)*rho_pcm*Qm*dt(solid)) from (dtube/2,0) to (dia/2,0)

HISTORIES

history(temp) at (.25*(dia/2-dtube/2)+dtube/2,0) (.5*(dia/2-dtube/2)+dtube/2,0) (.75*(dia/2-dtube/2)+dtube/2,0) export format
"#t,#r,#i"

history(solid) at (.25*(dia/2-dtube/2)+dtube/2,0) (.5*(dia/2-dtube/2)+dtube/2,0) (.75*(dia/2-dtube/2)+dtube/2,0) export format
"#t,#r,#i"

END

300 series simulation script

TITLE

'Foam/PCM Compositel'

COORDINATES

ycylinder('r','z')

SELECT

cubic

smoothinit

VARIABLES

temp(threshold=10)

solid(threshold=0.1)

DEFINITIONS

long = 0.0762	{ height of cylinder }
dtube = .0127	{ diameter of inner tube }
dia = 0.0889	{ diameter of foam/pcm }
ta=300	{ outside air temperature }
Qm= 251000	{ latent heat of the PCM J/kg }
Tm=329	{ Melting temperature }
T0= 10	{ Melting interval +- T0 }
temp_liq=300	{ initial liquid temperature }
temp_sol=300	{ initial solid temperature }
lambda = 42	{ Thermal Conductivity of the foam }
e=0.88	{ Porosity }
filled=1	{ fraction filled }
rhopcm=760	{ Density pcm kg/m3 }
cppcm=2000	{ heat capacity pcm - J/kg-- °C }
rhof=2200	{ Density solid ligaments of the foam - kg/m3 }
cpf=900	{ heat capacity -Foam -J/kg-- °C }
rceff= (e*filled)*(rhopcm*cppcm)+ (1-(e*filled))*(rhof*cpf)	{ effective heat capacity }
rhoeff= (e*filled)*(rhopcm)+ (1-(e*filled))*(rhof)	{ effective density }

INITIAL VALUES

temp=ta
solid = 0.5*erfc((temp-Tm)/T0)

EQUATIONS

temp: $rceff \cdot dt(temp) - \text{div}(\lambda \cdot \text{grad}(temp)) = (e \cdot \text{filled}) \cdot \rho_{pcm} \cdot Q_m \cdot dt(solid)$
solid: $dt(solid) = 100 \cdot (0.5 \cdot \text{erfc}((temp-T_m)/T_0) - solid) + 1e-8 \cdot \text{div}(\text{grad}(solid))$

BOUNDARIES

region 'Outer'

start 'outer' (0,-dia/2)

natural(temp)=-10*(ta-temp) { outer surface convection }

arc(center=0,0) angle 180

```

natural(temp)=0                                {cut line insulated}

line to (0, dtube/2)

natural(temp) = -24000*(368-temp)

arc(center=0,0) angle=-180

natural(temp)=0

line to close


FRONT(solid=0.5, 0.2)

TIME 0 by 1e-4 to 3600


MONITORS

for cycle=1

grid(r,z) zoom (0,-dtube,dtube,dtube)

elevation(Temp) from (dtube/2,0) to (dia/2,0) fixed range=(300,370) as "X-Axis Temp"

elevation(solid) from (dtube/2,0) to (dia/2,0) as "X-Axis Solid"

elevation(rceff*dt(temp), div(lambda*grad(temp)), rhoeff*Qm*dt(solid)) from (dtube/2,0) to (dia/2,0)


PLOTS

for cycle=10

grid(r,z)

contour( temp) fixed range=(300.0,370.0) painted

contour( temp) zoom (0,-dtube,dtube,dtube) fixed range=(300.0,370.0) painted

contour(solid) fixed range=(0.0,1.0) painted

contour(solid) zoom (0,-dtube,dtube,dtube) fixed range=(0.0,1.0) painted

grid(r,z) zoom (0,-dtube,dtube,dtube)

elevation(Temp) from (dtube/2,0) to (dia/2,0) fixed range=(300,370) as "X-Axis Temp"

elevation(solid) from (dtube/2,0) to (dia/2,0) as "X-Axis Solid"

elevation(rceff*dt(temp), div(lambda*grad(temp)), (e*filled)*rhoPCM*Qm*dt(solid)) from (dtube/2,0) to (dia/2,0)


HISTORIES

history(temp) at (.25*(dia/2-dtube/2)+dtube/2,0) (.5*(dia/2-dtube/2)+dtube/2,0) (.75*(dia/2-dtube/2)+dtube/2,0) export format
"#t,#r,#i"

history(solid) at (.25*(dia/2-dtube/2)+dtube/2,0) (.5*(dia/2-dtube/2)+dtube/2,0) (.75*(dia/2-dtube/2)+dtube/2,0) export format
"#t,#r,#i"

```

END

400 series simulation script

TITLE

'Foam/PCM Composite'

COORDINATES

ycylinder('r','z')

SELECT

cubic

smoothinit

VARIABLES

temp(threshold=10)

solid(threshold=0.1)

DEFINITIONS

long = 0.0762	{ height of cylinder }
dtube = .0127	{ diameter of inner tube }
dia = 0.0889	{ diameter of foam/pcm }
ta=300	{ outside air temperature }
Qm= 251000	{ latent heat of the PCM J/kg }
Tm=329	{ Melting temperature }
T0= 10	{ Melting interval +- T0 }
temp_liq=300	{ initial liquid temperature }
temp_sol=300	{ initial solid temperature }
lambda = 60	{ Thermal Conductivity of the foam }
e=0.83	{ Porosity }
filled=1	{ fraction filled }
rho_pcm=760	{ Density pcm kg/m3 }
cpcm=2000	{ heat capacity pcm - J/kg--°C }
rho_f=2200	{ Density solid ligaments of the foam - kg/m3 }
cpf=900	{ heat capacity -Foam -J/kg--°C }

$r_{\text{ceff}} = (e * \text{filled}) * (\rho_{\text{hopcm}} * c_{\text{ppcm}}) + (1 - (e * \text{filled})) * (\rho_{\text{h}} * c_{\text{pf}})$ {effective heat capacity}
 $\rho_{\text{heff}} = (e * \text{filled}) * (\rho_{\text{hopcm}}) + (1 - (e * \text{filled})) * (\rho_{\text{h}})$ {effective density}

INITIAL VALUES

temp=ta
 solid = 0.5*erfc((temp-Tm)/T0)

EQUATIONS

temp: $r_{\text{ceff}} * dt(\text{temp}) - \text{div}(\lambda * \text{grad}(\text{temp})) = (e * \text{filled}) * \rho_{\text{hopcm}} * Q_m * dt(\text{solid})$
 solid: $dt(\text{solid}) = 100 * (0.5 * \text{erfc}((\text{temp} - T_m) / T_0) - \text{solid}) + 1e-8 * \text{div}(\text{grad}(\text{solid}))$

BOUNDARIES

region 'Outer'

start 'outer' (0,-dia/2)
 natural(temp)=-10*(ta-temp) {outer surface convection}
 arc(center=0,0) angle 180
 natural(temp)=0 {cut line insulated}
 line to (0, dtube/2)
 natural(temp) = -24000*(368-temp)
 arc(center=0,0) angle=-180
 natural(temp)=0
 line to close

FRONT(solid-0.5, 0.2)
 TIME 0 by 1e-4 to 3600

MONITORS

for cycle=1
 grid(r,z) zoom (0,-dtube,dtube,dtube)
 elevation(Temp) from (dtube/2,0) to (dia/2,0) fixed range=(300,370) as "X-Axis Temp"
 elevation(solid) from (dtube/2,0) to (dia/2,0) as "X-Axis Solid"
 elevation($r_{\text{ceff}} * dt(\text{temp})$, $\text{div}(\lambda * \text{grad}(\text{temp}))$, $\rho_{\text{heff}} * Q_m * dt(\text{solid})$) from (dtube/2,0) to (dia/2,0)

PLOTS

for cycle=1

```

grid(r,z)

contour( temp) fixed range=(300.0,370.0) painted

contour( temp) zoom (0,-dtube,dtube,dtube) fixed range=(300.0,370.0) painted

contour(solid) fixed range=(0.0,1.0) painted

contour(solid) zoom (0,-dtube,dtube,dtube) fixed range=(0.0,1.0) painted

grid(r,z) zoom (0,-dtube,dtube,dtube)

elevation(Temp) from (dtube/2,0) to (dia/2,0) fixed range=(300,370) as "X-Axis Temp"

elevation(solid) from (dtube/2,0) to (dia/2,0) as "X-Axis Solid"

elevation(rceff*dt(temp), div(lambda*grad(temp)), (e*filled)*rho_pcm*Qm*dt(solid)) from (dtube/2,0) to (dia/2,0)

```

HISTORIES

```

history(temp) at (.25*(dia/2-dtube/2)+dtube/2,0) (.5*(dia/2-dtube/2)+dtube/2,0) (.75*(dia/2-dtube/2)+dtube/2,0) export format
"#t,#r,#i"

history(solid) at (.25*(dia/2-dtube/2)+dtube/2,0) (.5*(dia/2-dtube/2)+dtube/2,0) (.75*(dia/2-dtube/2)+dtube/2,0) export format
"#t,#r,#i"

```

END

Vita

Michael Trammell was born in Oak Ridge Tennessee on November 3, 1978. He grew up in Pioneer Tennessee and attended Jellico High School. After high school, he attended Pellissippi State Technical Community College where he graduated with an A.A.S in Mechanical Engineering Technology. He then attended East Tennessee State University and graduated with a B. S. in Manufacturing Engineering Technology. Michael is eagerly anticipating graduation from the University of Tennessee with a M.S. in Materials Science and Engineering.